J Mater Sci (2010) 45:3901–3911
DOI 10.1007/s10853-010-4450-3

# Machining damage analysis of alumina in relation to thermal shock behavior

**Ana L. Cavalieri · Norma Míngolo · Analía G. Tomba Martinez**

Received: 12 October 2009 / Accepted: 27 March 2010 / Published online: 13 April 2010


**Abstract** Machining damage of alumina disks with two different finishes, C and F, was analyzed with the aim of explaining the differences in their thermal shock responses. Thermal treatments designed to simulate conditions in thermal shock testing were performed on sets of C and F disks. The damage was quantified by several techniques, including the measurement of residual stresses. The mechanical strength of as-machined disks and thermally treated disks was also determined, including fractographic analysis. A decrease in the residual stresses after thermal treatment was observed in F specimens, as was expected. Conversely, unusual behavior was observed in C disks, showing a tendency to increase the residual stresses when the disks were kept at high temperature. Several factors were discussed to explain this fact. Higher mechanical strength and a decrease in the critical flaw size was observed in thermally treated disks compared to as-machined specimens for both types of finishes.

## Introduction

In spite of the several advantages ceramics possess—chemical inertia, refractoriness, and excellent mechanical properties at high temperatures—these materials are rather susceptible to damage or fracture under the thermal shock conditions they are subjected to while in service. Unfortunately, the great complexity of the material degradation under these conditions translates to the study of the thermal shock behavior.

Ceramic bodies for specific applications have to satisfy requirements of shape, dimensions, and surface quality. In spite of the relative difficulty and high cost, the machining of ceramics is the most common process used to meet these demands. In such a process, the material removal occurs by mechanisms of plastic deformation and brittle fracture, producing surface damage that includes flaws and residual stresses [1–8]. In this way, machining can strongly influence the strength of a component, and several works have been published regarding this issue [9, 10]. Moreover, this process also affects the thermal shock behavior of the material, although this topic has been studied less [11].

How this procedure modifies the flaw size distribution responsible for failure and what is the role of the residual stresses are the key issues with regard to the effect of machining on mechanical and thermomechanical behavior. Furthermore, effects of temperature on both flaw size distribution and the residual stress field must be considered [12–16]. However, none of these tasks is simple.

The final aim of this article is to explain the differences observed in the thermal shock response of alumina disks with two different surface finishes. Two sets of disks with a different surface finish were prepared and subjected to thermal treatments specifically designed to simulate the thermal conditions of thermal shock testing [11]. The machining damage of specimens before and after thermal treatments was analyzed employing several methods commonly used together: roughness parameters determination,

A. L. Cavalieri · A. G. Tomba Martinez
Instituto de Investigaciones en Ciencia y Tecnología de Materiales (INTEMA)-CONICET, Mar del Plata, Argentina

N. Míngolo
Centro Atómico Constituyente - CNEA, San Martín, Provincia de Buenos Aires, Argentina

A. G. Tomba Martinez (✉)
División Cerámicos-INTEMA, Fac. de Ingeniería, UNMdP, Av. Juan B. Justo 4302 (7600), Mar del Plata, Argentina
e-mail: agtomba@fi.mdp.edu.ar

SEM observation, X-ray diffraction, and mechanical testing (including fractographic analysis).

## Experimental procedure

### Preparation of specimens

Disks (diameter: 35.00 ± 0.02 mm, height: 2.68 ± 0.01 mm) were fabricated by slip casting of an aqueous suspension of a commercial high-purity alumina powder (Reynolds RC-HP DBM, $D_{50} = 0.35$ μm, $S_e = 7.3$ $m^2/g$). Green bodies were treated at 900 °C for 1 h and ground with SiC papers (120, 320, and 600 grit) before sintering at 1,600 °C for 2 h (heating rate of 2 °C/min). The density of the sintered material was 99.5% and its microstructure was found to be homogeneous, with equiaxial and elongated grains (mean size of 3.46 ± 2.27 μm) and few intergranular pores [10].

Two alternative abrasive treatments of one of the disk's plane surface were performed on sintered specimens: coarse machining (C) and fine machining (F). The C operation was carried out using a planetary grinding machine equipped with a resin-bonded diamond wheel (70 grit). The F finish was achieved with a semi-automatic polishing machine and SiC papers (120 and 320 grit).

### Thermal shock test

C and F disks were individually tested under thermal shock conditions [11]. The specimen was heated to a predetermined temperature ($T_i$) and cooled using a high-velocity air jet at room temperature ($T_0$) channeled onto the disk center for 20 s. After quenching, the specimen was cooled down, and if no cracking occurred, the temperature differential between the disk and the air jet was incremented by 10 °C until crack propagation was detected with the naked eye. The thermal shock resistance $\Delta T_C$, defined as the difference $T_C - T_0$, where $T_C$ is the value of $T_i$ when cracks are produced (crack initiation condition), was evaluated. Initial temperatures ($T_i$) in the 760–940 and 870–1,030 °C ranges were used for C and F disks, respectively.

### Thermal treatments

Thermal treatments simulating thermal shock conditions were performed on C and F disks. The experimental conditions were selected by considering those that could be supported by a disk having the experimental mean $\Delta T_C$ value in thermal shock tests. Every treatment was carried out in the thermal shock device.

C disks were successively treated in the following conditions (labels are in parenthesis): first, 760 °C, 90 min ($Ctt^1$); second, 810 °C, 450 min ($Ctt^2$); third, 940 °C, 21 h ($Ctt^3$). F disks, however, were successively subjected to the following thermal treatments (labels are in parenthesis): first, 870 °C, 90 min ($Ftt^1$); second, 1,030 °C, 25 h 30 min ($Ftt^2$).

### Surface characterization

Disks surfaces with ($Ctt^3$ and $Ftt^2$) and without (C and F) thermal treatments were examined by scanning electron microscopy (SEM), and their roughness was measured by profilometry. SEM analysis was performed with a Philips 505 equipment. Roughness measurements were carried out with a Surtronic 3+ (Taylor Hobson) profilometer with a diamond stylus (radius: 1 μm). On C and $Ctt^3$ surfaces, these measurements were done perpendicularly (⊥) and parallel (∥) to the direction of the machining grooves.

### Residual stresses measurements

The residual stresses ($\sigma_R$) of the disks were measured by X-ray diffraction (XRD). Values of $\sigma_R$ in C and F specimens before and after each respective step of thermal treatment were measured. Values of microstrain (με) and microstress were also determined as another measurement of the machining damage [4, 17].

The X-ray diffraction patterns on the surfaces of as-sintered, as-machined (C and F), and thermally treated disks ($Ctt^3$ and $Ftt^2$) were obtained in order to characterize the crystalline structure. The experimental patterns were measured with a Philips PW3710 diffractometer using Cu$K\alpha$ radiation ($\lambda = 0.15{,}406$ nm) and a Ni filter, with a penetration depth of approximately 16.8 μm for alumina. The diffractometer was operated at 40 kV and 30 mA, and the range of $2\theta$ was from 20° to 120° using a $2\theta$-step of 0.02° at 1 s per step.

Residual stresses were determined using the conventional $\sin^2\psi$ method, and microstrains were obtained from the broadening of diffraction peaks. The measurements were carried out at three different positions on the machined disk surface (at the centre and at two aligned points, each one at ≈8 mm from the disk periphery) using a Rigaku-Strainflex MSF-2M equipment. Cr$K\alpha$ radiation ($\lambda = 0.22896$ nm) and a V filter, with a penetration depth of about 8 μm for alumina, were used for the measurements. The diffraction peaks were registered in the range 120°–150° for $2\theta$, with a 0.02° $2\theta$-step at 8 s per step. Ten values of the $\psi$ angle, which is defined between the normal to sample and the normal to $\{hkl\}$ diffracting plane, were selected from 0° and 70°. The diffraction intensities for a fixed $\psi$ angle were measured for {1 0 10} and {1 1 9} alumina planes. The experimental diffraction patterns were fitted using the Rietveld method [18] to obtain a better

resolution for determining peak positions (macrostress) and peak broadening (microstrain).

Even when there was a directional pattern in the surface of the C disks, residual stress determination was carried out in random orientations with respect to the machining grooves since the thermal shock conditions used here did not discriminate between grinding directions.

### Mechanical testing

Disk fracture strength ($\sigma_F$) at room temperature with ($Ctt^3$ and $Ftt^3$) and without (C and $F^{10}$) thermal treatment was evaluated in biaxial flexure, employing a loading ball (8.04 ± 0.02 mm in diameter) on a discontinuous ring fixture (19.50 ± 0.1 mm in diameter, 12 balls in contact) [12]. The tests were performed in a servohydraulic testing machine Instron model 8501, with displacement control (0.05 mm $min^{-1}$).

The fracture characteristics of broken disks were analyzed. Crack patterns were optically inspected (with the naked eye and using a 1.5× magnifying glass). Fracture surfaces were studied by SEM (Philips 505) according to the procedure given in ASTM-C 1322/96 [19].

## Results

The values of $\Delta T_C$ obtained from the thermal shock tests of alumina specimens with C and F surface treatments were 765 ± 51 and 916 ± 54 °C, respectively [11]. These results show that the thermal shock behavior depends on the surface finish.

The general aspect of $Ctt^3$ and $Ftt^2$ surfaces observed by SEM (Fig. 1) was very similar to that observed for C and F specimens, respectively [10]. Pronounced machining grooves with a well-defined orientation were observed in C and $Ctt^3$ disks, while the action of abrasive grains in the fine wear (F and $Ftt^2$) did not leave a directional pattern. A lot of cavities together with smooth zones were identified on every surface. The microstructure of F surfaces was more homogeneous than those of coarse ground ones. We concluded that the mechanisms of brittle fracture and plastic deformation made a distinct relative contribution, with the latter being higher in C disks than in F disks.

Some of the roughness parameters values are reported in Table 1 [10]. All of the roughness parameters that measure the size (Ra, Rp, Rv, Rt, Rpm, RzDIN) as well as the frequency (RS, RSm) of the surface irregularities (the most relevant shown in Table 1) decreased with thermal treatment in both kind of surface finishes, being more pronounced in F disks.

The XRD pattern obtained with Cu$K\alpha$ radiation for as-sintered specimens showed the trigonal alumina structure (99.93 wt%), as determined by Rietveld refinement. The differences observed in the XRD patterns of other disks (C, F, Ctt3, and Ftt2), were attributable to $2\theta$-peak position (lattice parameters) and peak broadening (microstrain) variations. From the Rietveld refinement results, texture

**Table 1** Roughness parameters

| | As-sintered | C | | $Ctt^3$ | | F | $Ftt^2$ |
|---|---|---|---|---|---|---|---|
| | | ⊥ | ∥ | ⊥ | ∥ | | |
| Ra (μm) | 0.19 | 0.72 | 0.66 | 0.42 | 0.37 | 0.51 | 0.23 |
| Rt (μm) | 1.86 | 5.98 | 5.75 | 3.03 | 3.12 | 5.56 | 2.21 |
| RzDIN (μm) | 1.37 | 5.13 | 4.62 | 2.54 | 2.39 | 4.36 | 1.74 |
| RS (μm) | 14.80 | 18.30 | 21.30 | 10.20 | 10.80 | 18.90 | 7.40 |

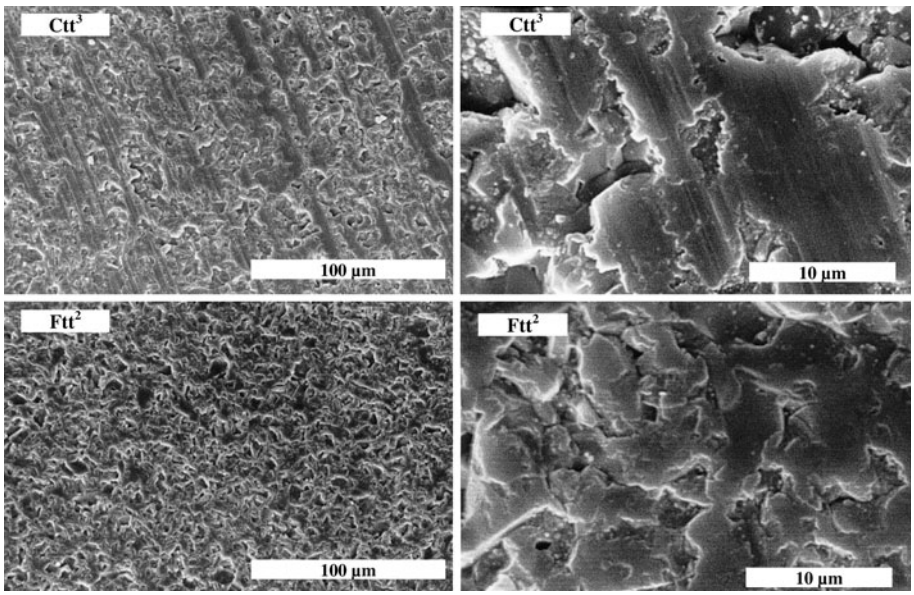


**Fig. 1** SEM micrographs of machined surfaces after thermal treatments

coefficient values, as a relative indication of the preferred orientation, were calculated using the relation between the measured intensity and the intensity obtained from a standard reference (JCPDS 46-1212) of each (*hkl*) reflection in the diffraction pattern. For every analyzed disk, the coefficient was around unity, showing that (1 0 10) and (1 1 9) planes used for residual stress evaluation did not exhibit preferred orientation.

The experimental conditions selected for residual stress determination by X-ray diffraction (described in "Experimental procedure" section) were suitable to discriminate (1 0 10) and (1 1 9) $2\theta$-peak positions at each angle $\psi$. Values of $\sigma_R$ were calculated using the following equation:

$$\sigma_R = -K_i m, \tag{1}$$

where $m$ is the slope of the straight line of $2\theta$ versus $\sin 2\psi$ plot and $K_i$ is a constant obtained from Eq. 2:

$$K_i = \frac{\cot g\theta\pi}{360\frac{1}{2}S_2}. \tag{2}$$

The crystallographic elastic constants (½ $S_2$) were calculated using the Reuss approach [20] and considering the single crystal elastic constants corresponding to the orientation of diffracting plane [21]: 3.1283 and 2.8139 T $Pa^{-1}$ for (1 1 9) and (1 0 10) planes, respectively. The values obtained for $K_i$ were: −1,127 and −1,285 (MPa/°) for (1 1 9) and (1 0 10) planes, respectively.

The accuracy of the stress results depends on several factors. The average error in the determined peak positions in $2\theta$ and the residual stress results were less than 0.005° and 10%, respectively, for all measurements.

Typical $2\theta$ versus $\sin^2\psi$ experimental data, together with the linear fit, are plotted in Fig. 2 for C disks. Average values (three samples and three results for each sample in the same conditions) of residual macrostresses ($\sigma_R$) and microstrains ($\mu\varepsilon$) for as-sintered C and F samples [10] and thermally treated disks are plotted in Figs. 3 and 4. Residual

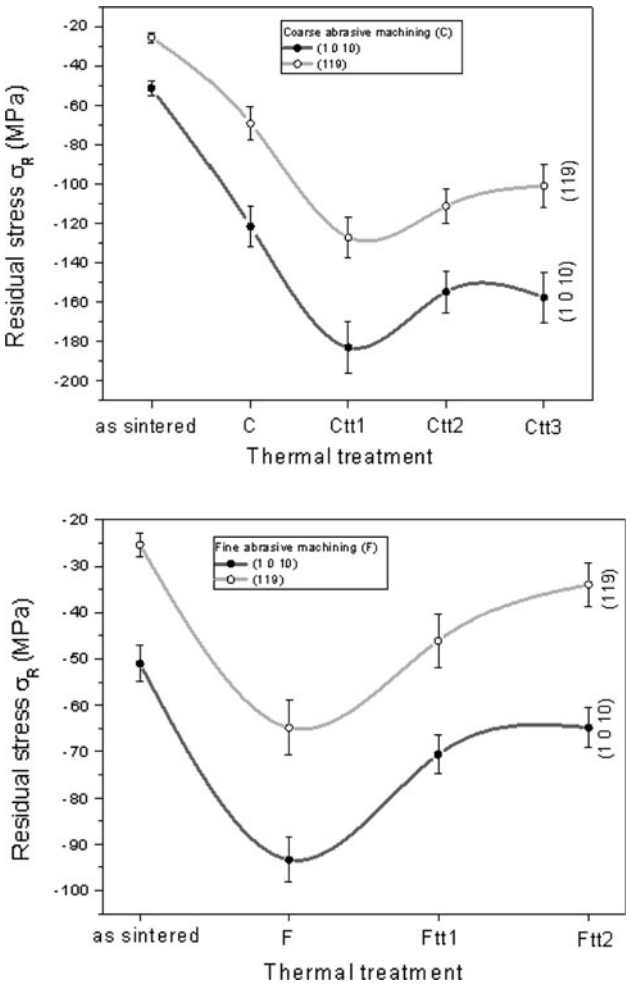


**Fig. 3** Distribution of residual stresses for thermal treatments

macrostresses were compressive for both crystallographic planes in every case, including the as-sintered condition. In reference to the as-sintered disks, both surface finishes increased the compressive residual stress in the order C > F [10].

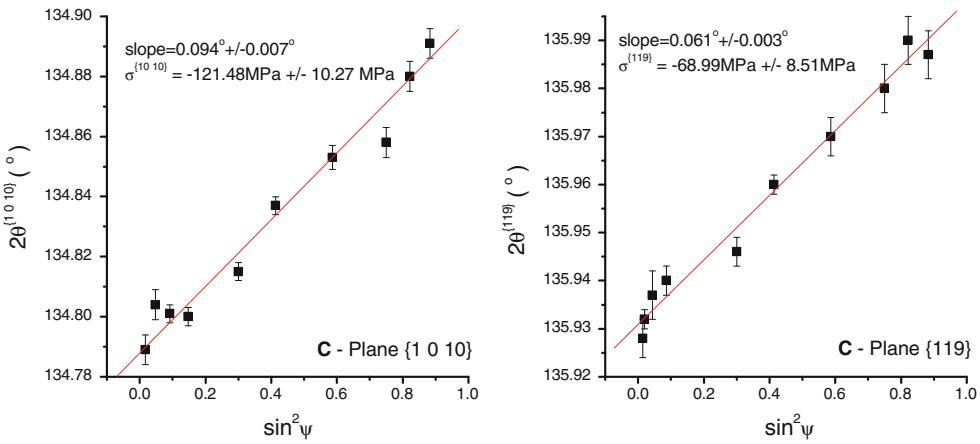


**Fig. 2** $2\theta$ versus $\sin^2\psi$ data and linear fitting for C disk

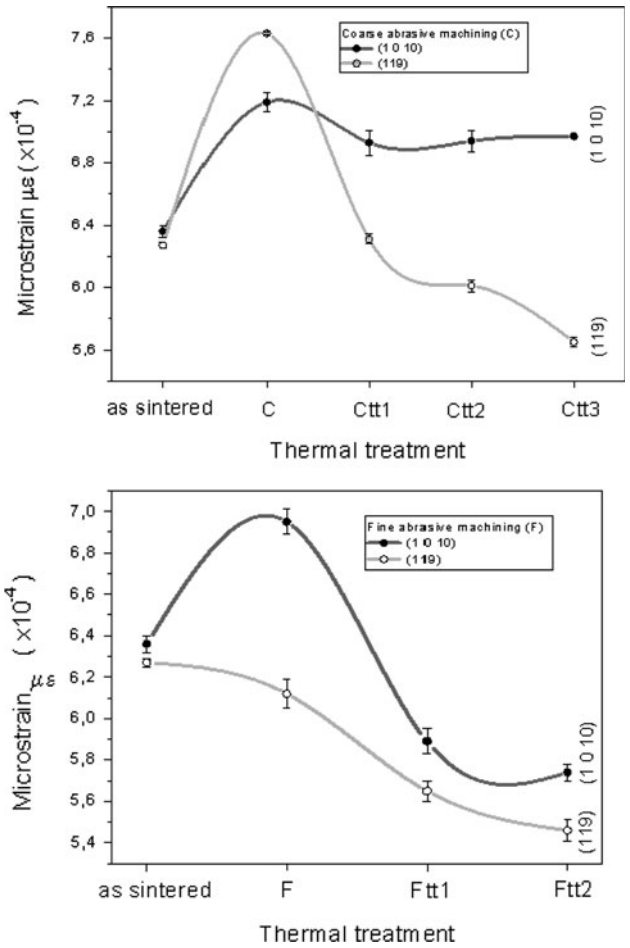


**Fig. 4** Distribution of microstrains for thermal treatments

The effect of the thermal treatments was different in each type of surface finish: a relief of residual stresses was determined for F disks while an unexpected tendency to increase $\sigma_R$ was observed in C specimens. In the latter, even when a decrease of the average $\sigma_R$ was observed after the second and third thermal treatments, the values were always greater than the initial condition (C). In addition, some of the individual specimens still exhibited an increase in residual stresses. For F disks, it was also observed that the distribution of residual stresses for the three points measured in each sample was rather uniform. For C disks, however, deviations less than 10% with respect to the average values obtained for each sample were observed. The higher scattering of $\sigma_R$ for C disks was attributed to the dependency on grinding direction, which was not considered in residual measurements.

On the other hand, the values of microstrains increased after machining operations. Disks with coarse machining reached the highest deformations. Thermal treatments produced a decrease in the microstrain values of C and F disks, with a more pronounced decrease in the latter. The magnitude of microstrains after each thermal treatment slightly decreased for the C disks (Fig. 4), but they were still elevated compared to the as-sintered reference specimen.

**Table 2** Fracture parameters

| | C | Ctt[3] | F | Ftt[2] |
|---|---|---|---|---|
| *Biaxial flexure* | | | | |
| $\sigma_F$ (MPa) | 296 ± 59 | 485 ± 11 | 220 ± 66 | 329 ± 84 |
| Origin[a] | | | | |
| $c$[b] (μm) | 159 ± 43 | 79 ± 16 | 137 ± 23 | ~30 |
| $c/2a$[c] | 1.0 ± 0.3 | ~2.0 | 1.1 ± 0.1 | ~1.5 |
| $c_{calc}$ (μm) | 294 | 92 | 558 | 131 |
| Mode of fracture[c] | I(↑) + T | I(↑) + T | I + T | I(↑) + T |
| *Thermal shock* | | | | |
| Mode of fracture[c] | I(↑) + T | – | I(↑) + T | – |

*I* intergranular, *T* transgranular

[a] The largest flaw was considered for associated defects

[b] $c$: major axis of the elliptical flaw

[c] $a$: minor semi-axis of the elliptical flaw

Values of mechanical strength are reported in Table 2 [10, 22]. An increment in strength for C specimens (≈22%) was observed compared to the mechanical strength of as-sintered disks, 243 ± 30 MPa. The slight decrease of the mean strength for disks with F finish (≈10%) was not considered significant. After the thermal treatments, $\sigma_F$ values for both machined specimens increased (in proportions of 64% for C disks and 50% for F disks). The fragmentation of Ctt[3] and Ftt[2] specimens tended to be higher than those exhibited by as-machined disks (C and F, respectively). The number of fragments was only 2–3 for C and F disks and 3–5 for thermally treated specimens. No significant differences were observed in the branching features of thermally treated disks (Ctt[3] and Ftt[2]) with respect to those of C and F disks [10, 22].

Table 2 also summarizes the results obtained from the fractographic analysis of the different types of specimens [22], including those subjected to thermal treatments. In the latter, the fractographic analysis was rather hard to perform due to the irregularity of edge between the machined surface and the fracture surface of the disks. Furthermore, a high degree of flaw association was detected in these thermally treated disks (more than in C and F disks), so it was difficult to identify which of them acted as the fracture origin. Even though these defects tended to be elliptical, they were rather irregular in shape and their size was difficult to determine. SEM micrographs of fracture surfaces of Ctt[3] and Ftt[2] specimens are shown in Figs. 5 and 6.

The average sizes ($c$ and $a$) of those flaws considered as fracture origins of Ctt[3] and Ftt[2] were smaller in comparison with C and F disks, respectively. It was also evident from

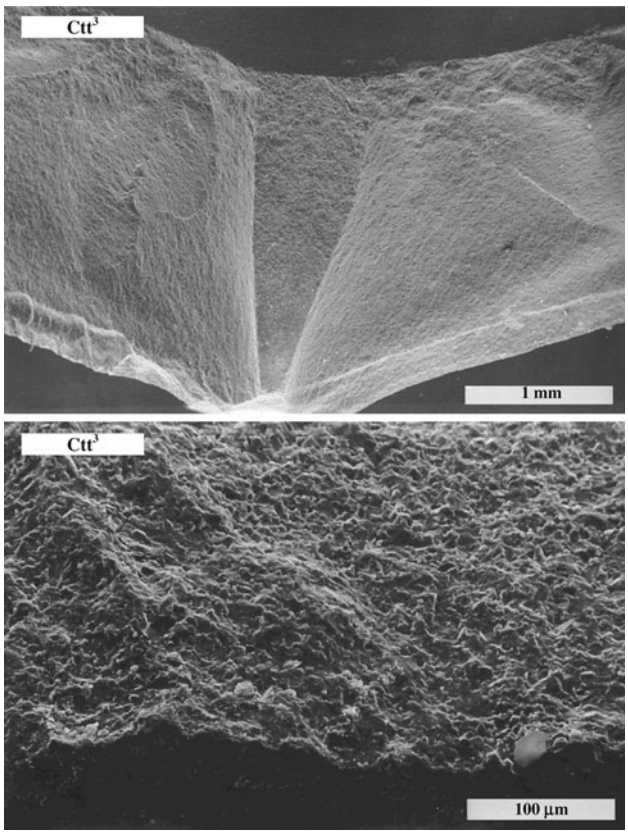


**Fig. 5** SEM micrographs of fracture surfaces of $Ctt^3$ disks

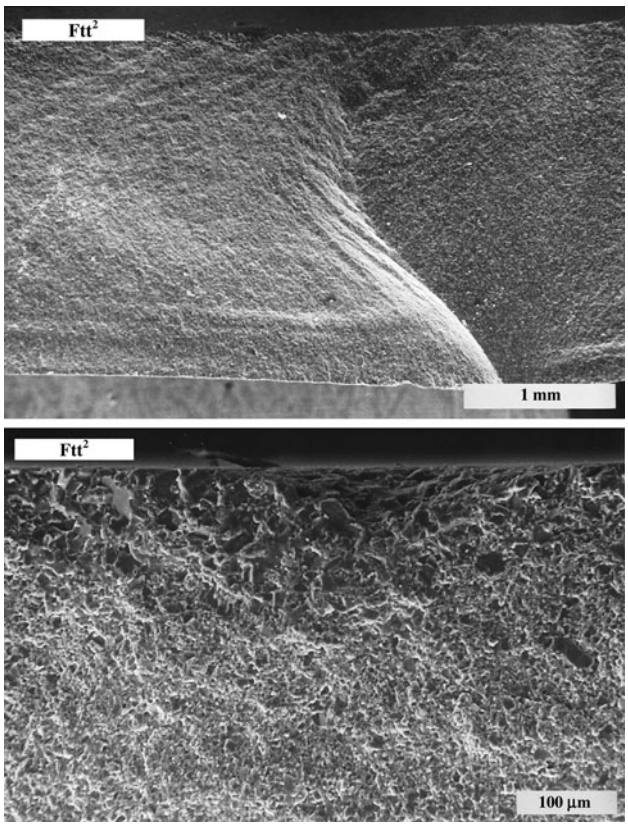


**Fig. 6** SEM micrographs of fracture surfaces of $Ftt^2$ disks

SEM images that the flaws in thermally treated specimens tended to be shallower, with a higher $c/2a$ ratio.

No fracture pattern could be identified in $Ctt^3$ and $Ftt^2$ disks and a mixture of intergranular and transgranular fractures was observed, with a higher contribution of the first mode. Compared with C and F disks, the contribution of intergranular failure was even higher and the fact that fracture surface irregularities was smaller attracted attention.

## Discussion

Considering the properties of as-sintered disks, both C and F finishing operations introduce surface and sub-surface damages. Moreover, features of machined surfaces observed by SEM and surface roughness suggest different mechanisms of material removal in those grinding procedures. Considering macrostress and microstrain values, a higher amount of machining damage in C disks can be inferred. These facts were attributed to the combination of several factors concerning each machining operation [10]: abrasive material hardness, abrasive grain size, temperature reached during the process [9], operative variables (grinding force, infeed, etc.).

### Surface characteristics

In the analysis of the effect of thermal treatments on the surface characteristics of C and F disks, only roughness parameters showed detectable changes. All the parameters diminished with thermal treatments and the disks showed a decrease in surface irregularities (in depth and frequency), that is attributed to the tendency of the system to reduce the surface free energy.

### Residual stresses

After the stay at high temperature, the expected relief of compressive residual stresses was observed in the sub-surface region of F specimens ($\approx$8 µm). The successive exposures to temperatures within the range of 870–1,030 °C for long time durations (27 h) had effects equivalent to annealing for this type of alumina material [12–16]. Nevertheless, complete relief was not achieved, with values of $\sigma_R$ being slightly higher than those of as-sintered disks. In turn, an unexpected tendency toward higher values of compressive residual stress was obtained after the thermal treatments of C disks (760–940 °C, 30 h). The repeatability of $\sigma_R$ values between the three specimens

and the mechanical response of Ctt[3] disks, which will be discussed later, give credit to the measurements.

A possible explanation for the behavior of C disks is based on the alteration of the compressive stress distribution along the disk height (depth) with temperature. It has been reported [23] that severe machining procedures lead to compressive residual stress profiles where the maxima level is not at the sample surface but in any layer in the sub-surface region (up to 20 μm). In a first approximation, X-ray diffraction patterns using Cu$K\alpha$ and Cr$K\alpha$ radiation (with different penetration depths) were used to get information about the residual stresses variation through the depth without removing layers of material. The interplanar spacing ($d_{hkl}$) and microstrain ($\mu\varepsilon_{hkl}$) obtained for the (1 0 10) and (1 1 9) planes, parallel to sample surface (at $\psi = 0^{o}$) are reported in Table 3. Considering that the value $d^{o}_{hkl}$, is the interplanar spacing for standard alumina free-stress, the residual stress is compressive if $d_{hkl} > d^{o}_{hkl}$ and tensile if $d_{hk} < d^{o}_{hkl}$. The data in Table 3 show different distributions of residual compressive stresses between the C and Ctt[3] disks. With respect to C disks, a smaller level of compressive residual stress was determined with Cu$K\alpha$ radiation in Ctt[3] disks, showing a partial relaxation of stresses. Moreover, the distribution of residual stresses in Ctt[3] specimens seemed to be more uniform along the evaluated depth. At this depth ($\approx$17 μm), neither the total relaxation of residual stresses nor the change to tensile stresses had been produced yet. The alteration of the residual stress gradient along the depth after thermal treatments can be attributed to microstructural changes (changes in density and size of flaws and pores, for instance) introduced by temperature on the layer affected by the coarse machining.

Besides the residual stress redistribution produced by temperature, it is important to note that the magnitude of $\sigma_R$ is a mean value obtained by integration over the volume determined by the irradiated area and the depth of X-ray penetration (Cr$K\alpha$ radiation in our case). Considering that the maximum level of compressive stress in C disks occurs at a layer located deeper than the near-surface region where Cr$K\alpha$ penetrates (Table 3), the overall residual stresses in C disk could be underestimated. Furthermore, it is possible that the stress level is reduced by the effect of temperature, but at the same time, the maximum value approaches the surface. In this way, the stress average in the evaluated volume could turn out higher after thermal treatment.

Another aspect that could explain the stress behavior in C disks is the influence of the dislocation zone depth in relation to residual stresses. In machined specimens, any residual stress is the result of local plastic deformation, and it is reasonable to assume that compressive stresses only extend to a depth related to the dislocation zone depth [24]. Wu et al. [25] assume, in a simple approximation, that the residual stress distribution beneath the surface can be described by a simple step function in which the compressive stress is confined to a region with a high dislocation density. Below this, there is a much larger region in which there is counterbalancing tensile stresses.

Based on this interpretation, the depth of compressive residual stress ($d$) can be changed with the depth and distribution of the dislocation density zone generated by coarse (C) or fine (F) machining. In general, the lack of dislocation mobility limits the relaxation of residual stresses imposed under abrasive conditions. Choi et al. [26] reported that dislocation movements are possible in single crystal alumina at temperatures ranging from 600 to 1,400 °C by plastic slip, which could influence the microstrain at grain scale. In polycrystalline alumina, diffusion-driven grain boundary sliding may also be an important deformation mechanism [27] that could influence the macrostrain. Thus, thermal conditions of the first treatment of C disks (760 °C, 90 min) may not be enough to produce an efficient mobility of dislocations to alleviate the residual stresses and then reduce the strained layer. At higher temperature and time durations, the dislocation movement and residual stress relief are facilitated, which

**Table 3** Interplanar spacing ($d_{hkl}$) and microstrain ($\mu\varepsilon_{hkl}$) for different X-ray penetration depth ($\psi = 0°$)

| ($h$ $k$ $l$) | λCu$K\alpha$-radiation (17 μm) | | λCr$K\alpha$-radiation (8 μm) | |
|---|---|---|---|---|
| | $d_{hkl}$ (Å) | $\mu\varepsilon_{hkl}$ ($\times 10^{-4}$) | $d_{hkl}$ (Å) | $\mu\varepsilon_{hkl}$ ($\times 10^{-4}$) |
| As-sintered | | | | |
| (1 0 10) | 1.23930 ± 0.00002 | 5.91 | 1.23899 ± 0.00002 | 6.36 |
| (1 1 9) | 1.23440 ± 0.00006 | 5.88 | 1.23405 ± 0.00005 | 6.27 |
| C | | | | |
| (1 0 10) | 1.23950 ± 0.00002 | 6.42 | 1.23910 ± 0.00002 | 7.19 |
| (1 1 9) | 1.23470 ± 0.00004 | 6.40 | 1.23413 ± 0.00006 | 7.63 |
| Ctt[3] | | | | |
| (1 0 10) | 1.23920 ± 0.00001 | 5.56 | 1.23920 ± 0.00003 | 6.97 |
| (1 1 9) | 1.23430 ± 0.00003 | 5.54 | 1.23420 ± 0.00007 | 5.65 |

Tabulated values of interplanar spacing $d^{hkl}_{o}$ for standard alumina free-stress

$d^{o}_{1\ 0\ 10} = 1.23890$ Å

$d^{o}_{1\ 1\ 9} = 1.23390$ Å

could also contribute to the reduction of residual stress levels in $Ctt^2$ and $Ctt^3$ disks.

An estimation of the compressive residual stress depth can be obtained for the as-machined (C and F) and thermally treated disks ($Ctt^3$ and $Ftt^2$) by using the expression [9]:

$$d = 0.7^{1/3}(\mathrm{RzDIN})^{2/3}\left(\frac{E}{H_v}\right)^{2/5}, \quad (3)$$

where $r$ is the mean radius of the abrasive grain (46 μm for F and 160 μm for C) and RzDIN is taken in the direction perpendicular to that of the machining grooves. Room temperature values of the Young modulus ($E = 380$ GPa [28]) and Vickers hardness ($H_V = 20$ GPa [29]) for the calculus were taken from literature. In the same way, reported values of $E$ (250GPa) and $H_v$ (8GPa) in the range 900–1,000 °C [30] were employed for the estimation of the depth in thermally treated specimens ($Ctt^3$ and $Ftt^2$).

Estimated values of $d$ were: 37, 28, 22, and 14 μm for C, $Ctt^3$, F, and $Ftt^2$, respectively. The higher $d$ calculated for C disks with respect to F disks is consistent with the higher damage degree inferred for the former type of disks. In turn, a decrease in the region subjected to residual compressive stresses (lower depth) was observed in thermally treated disks ($Ctt^3$ and $Ftt^2$). These results are in agreement with both the residual stress distribution and its changes with temperature for C disks, as mentioned earlier.

The contribution of the different macro-microstructural factors (stress gradient, dislocations, roughness, flaws/pores), which is believed to explain the residual stress evolution in C disks with thermal treatment, is difficult to be quantified. Nevertheless, any of them could account for the experimental data for coarse machining disks and the effect of the permanence at high temperature.

## Microstrains

The evolution of microstrain during thermal treatment was similar for both types of surface finishes (Fig. 4). Both machining operations increased the microstrain with respect to the as-sintered condition due to microplastic deformation occurring in the near-surface regions. The evolution of microstrain in F disks after thermal treatment ($Ftt^1$ and $Ftt^2$), which resulted in values lower than those obtained for "as-sintered" disks, is consistent with the decrease in roughness, the movement of dislocation favored by temperature and the residual stresses relaxation.

Conversely, even when the microplastic deformation was reduced with temperature in C disks, the level of microstrain remained a little higher than those measured in the as-sintered condition. Similar considerations regarding the macrostress evolution of C disks could be used to explain the microstrain levels. It is important to note that macroscopic residual stress measurements are related to the deformation between different grains in the average volume exposed to the X-ray and have statistical meaning. However, these measurements do not take into account microscopic local variations as could occur in density or size of flaws or dislocations, which can affect the microstrain measurements from the X-ray peak broadening. The distribution of microstrain in Table 3 indicates the presence of a gradient along the depth. The decrease of $\mu\varepsilon$ far away from the sub-surface region ($\approx 17$ μm) can be associated with a low level of microplastic deformation.

## Mechanical behavior

In the analysis of the mechanical response of alumina disks with different machining and thermal treatments, several factors should be considered: residual stresses, depth affected by stress, and flaw sizes [9, 31, 32]. All of these factors are related to each other and are influenced by exposure to high temperature. Thus, the panorama is rather complex. The effect of the superposed compressive residual stresses on a material under mechanical loading could be positive since the opening force acting on the superficial or sub-surface flaws would be reduced [9]. However, the magnitude of this effect depends on the relation between the flaw size and the depth of compressive residual stresses.

From the experimental values of mechanical resistance, the size of critical flaws acting as the fracture origin ($c_{calc}$) was estimated (Table 2). For the calculus, the following expression [17] was used:

$$c_{calc} = \left(\frac{K_{IC}}{\sigma_0 Y}\right)^2. \quad (4)$$

The nominal stress $\sigma_o$ was calculated as the sum of $\sigma_F$ and $\sigma_R$, and the shape factor ($Y$) values corresponding to each relation $c/2a$ were extracted from literature [33] (C and F: 1.30; $Ctt^3$: 1.24, $Ftt^2$: 1.29). A value of $K_{IC}$ for alumina [33] corrected by porosity (0.5%) [34] of 3.9 M $Pam^{1/2}$ was used.

The increment of $\sigma_F$ of C disks with respect to that of as-sintered specimens stems from the presence of compressive residual stresses coming from the machining, which have quite higher magnitudes and greater depths than those generated during sintering. The type of defect identified as the fracture origin exhibited an approximately semi-elliptical shape, with a high degree of association, typical of machining damage [22]. The difference between fractographical flaw size and $c_{calc}$ is partially attributed to the high degree of association. This phenomenon tends to reduce the stress intensity factor in the area surrounding the defect [33] and makes it difficult to assign just one flaw

size for a set of defects. On the other hand, the value of the ratio $a/d$ was $\approx 2$ for C specimens, and because of this, the contribution of residual compressive stresses is partial (only a portion of the defect is submerged in the residual compressive zone).

In the case of disks with F finish, the mechanical strength was unchanged with respect to as-sintered disks. This fact was accounted for considering that the flaw size $a$ was up to $\approx 3$ times the value of $d$ for this type of disk. In this way, the effect of the compressive residual stress on the crack is low. With regard to fracture features, the defects identified as fracture origins were those typical of machining procedures [33], but without association. In the case of F finishing, the difference between calculated and experimental flaw sizes was higher than in C disks. This fact is attributed to the higher difference between $a$ and $d$ in fine ground specimens, since the defect association was not evident in this case.

With regard to the thermal effect on the mechanical strength, the large increment in $\sigma_F$ observed in C is consistent with the increase registered in the average residual stresses. On the other hand, the value of $a/d$ for $Ctt^3$ was 0.7 (rather lower than the ratio for C disks), showing that critical flaws were completely submerged in the compressive residual stresses region. Due to this fact, the presence of compressive residual stresses was very effective for reducing the nominal stress. Moreover, the similarity between the experimental and calculated values of $c$ for $Ctt^3$ disks lends support to this reasoning. Thus, the presence of compressive residual stresses is considered the main cause for the mechanical strength of coarse machined disks.

The reduction of the size of defects in $c$ ($\approx 50\%$) as well as in $a$ parameters, and the tendency to a higher ellipticity (higher $c/2a$) in $Ctt^3$ disks with respect to as-machined disks would imply that the time passed at high temperature led to a healing or closure of defects, as reported in other systems [35–37]. This phenomenon could occur by bulk and/or grain boundary diffusion [36, 37]. The tendency of the major axis $c$ to diminish in a greater degree than the minor axis $a$, could be attributed to differences in the energy content between the atoms at the surface and those located within the bulk of the material.

The mechanical behavior of fine ground specimens was different from that of C specimens when taking into account that a relief of residual stresses occurred after each thermal treatment. Furthermore, a value of 0.7 was estimated for the $a/d$ ratio in $Ftt^2$ disks, showing that the flaws were completely embedded into the region of compressive residual stresses. Based on these facts and the levels of residual stresses exhibited by F disks, it is considered that in this case, the small flaw size is dominating the mechanical behavior. This reasoning also explains the discrepancy between the experimental value of $c$ and $c_{calc}$.

As in coarse machined specimens, the increment in the values of $c$, $a$, and $c/2a$ implies that healing of cracks could also be produced in $Ftt^2$. In this case, the reduction of $c$ was even higher (78%), which is attributed to the high temperature and times employed in the thermal treatments for this type of disks.

From fractographic data, a change of crack size distribution after thermal treatments can be inferred. As was mentioned before when the evolution of compressive residual stresses in C disks was discussed, this alteration could affect residual stress determinations since the stress distribution through the depth is not as simple as the model proposed by Wu et al. [25], and it also depends on the crack depth ($a$).

The tendency to increase the fragmentation and the intergranularity in the fracture of both types of specimens (coarse and fine machined disks) after each thermal treatment has an explanation similar to that of the differences between failure in thermal shock conditions and in biaxial flexure [22]. Since thermally treated disks failed at a higher value of nominal stress $\sigma_o$ than as-machined specimens, the stored mechanical energy was also higher.

## Thermal shock behavior

Finally, the effect of thermal treatments, which have the objective of simulating those involved in thermal shock tests on C and F disks should be used to explain the disks' behavior under thermal shock conditions. Experimental results show that C specimens with higher mechanical strength (at room temperature) and compressive residual stresses are those less resistant to thermal shock, even taking into account the effect of thermal treatments on $\sigma_R$ and $\sigma_F$. Possible explanations were proposed [11]: the higher convective heat transfer coefficient determined in C specimens [38, 39] and the alteration of residual stresses during successive tests (the influence of the thermal dependence of mechanical properties was not considered significant due to little change up to 1,100 °C for alumina materials [11, 29]). Taking into account the results in other materials subjected to similar thermal shock tests [40], which indicate that temperature is the main cause of the modification of residual stresses, ad hoc thermal treatments were designed for C and F disks in order to clarify the importance of this factor in this cases. However, the obtained results show that the re-distribution of residual stresses by thermal effect that actually occur do not alter the relative order of mechanical resistance between C and F disks. In this manner, the alteration of residual stresses does not explain by itself the thermal shock behavior of both types of specimens.

Another factor that could change the thermal stress distribution in this type of tests is the quenching itself,

which could produce stress relaxation as already reported [23]. In this case, it is possible that the redistribution of residual stresses by thermal effects overlaps with that produced by the air impingement. It is expected that the addition of both factors accelerates the reduction in the residual stress level. If this overlapping indeed occurs, and taking into account that machining flaws of F disks tends to be smaller than those of C specimens (even considering that healing could also happen), it is possible that the flaw size becomes the factor limiting mechanical resistance when few or no residual stresses are counteracting thermal stresses. If so, fine ground disks could be more resistant to thermal shock conditions.

Finally, a factor that could cause the different thermal shock behavior of C and F specimens is that the machining damage, mainly cracks, may alter the local heat flow in the sub-surface region of disks (which is the basis of the "thermal wave measurement" to evaluate sub-surface damage [7, 41]). High flaw density decreases the thermal diffusivity because they act as barrier to thermal waves [7, 41]. In the thermal shock test used in this research, the maximum tensile stress occurs in the surface region, which makes the heat transfer in this region critical. If it is assumed that higher surface damage leads to lower thermal diffusivity (and, in consequence, a lower thermal conductivity), the thermal shock will be more severe since greater stress will be developed. This is the same effect produced by a higher superficial thermal transfer coefficient. This factor could contribute to decrease the thermal shock resistance of C disks, with higher levels of surface and sub-surface damage, with respect to F specimens.

Unfortunately, the results with regard to the residual stress evolution in relation to thermal shock behavior are open to more than one interpretation, and the overall picture is not completely clear. For a better knowledge of the macroscopic residual stresses behavior in different layers affected by machining, in the further work is considered the evaluation of the residual stress profile in depth using Cr$K\alpha$ radiation after removing stepwise thin surface layers by a high-quality polishing process, which results in additional small residual stresses [42].

## Conclusions

The evaluation of the thermal shock behavior of alumina disks with different surface finishes, coarse abrasive machining (C) and fine abrasive machining (F), showed that the values of $\Delta T_C$ depended on the surface finish. In order to explain this fact, C and F disks were subjected to thermal treatments specifically designed to simulate the thermal conditions of thermal shock testing. The machining damage of specimens before and after thermal treatments was analyzed employing several methods. The results obtained from the correlation of the several measured parameters and its variation with thermal treatments have some interesting implications. The main conclusions of the work are as follows.

- The thermal treatments did not change the general aspect of the surface microstructure in any of the disks and only the roughness parameters showed a significant decrease that was attributed to the tendency of the system to reduce the surface free energy.
- A decrease in the compressive residual stresses ($\sigma_R$) after thermal treatment was observed in F specimens, as was expected, while unusual behavior was identified in C disks, which showed a tendency to increase the values of $\sigma_R$ as the staying of the disks at high temperature was longer; several factors were discussed to explain this fact: the alteration of the compressive stress distribution along the disk height (depth) with temperature, a possible underestimation of the overall residual stresses in C disk (taken as reference), the influence of the dislocation zone depth in relation to the depth of compressive residual stresses.
- Higher mechanical strength ($\sigma_F$) and a decrease in the critical flaw size (crack closure) was observed in thermally treated disks compared to as-machined specimens for both types of finishes; in C disks, this is consistent with a mechanical behavior dominated by the compressive residual stresses while the small flaw size limited the response of thermally treated F disks.

However, even when the results showed an alteration of residual stresses by thermal effects, they did not explain by theirself the thermal shock behavior of both types of specimens, and other factors have to be taken in account as the influence of the air impingement itself on the residual stress distribution and the effect of cracks on the thermal diffusivity. Even so, the obtained results gave a more detail description of the complex panorama of thermal shock condition. Moreover, they also confirmed the complexity associated with the machining procedure, which is a multivariable problem with technological implications, and the difficulty in making general guidelines for the machining of ceramic components in relation to the in-service conditions.

## References

1. Marshall DB, Evans AG, Khuri Yakub BT, Tien JW, Kino GS (1983) Proc R Soc Lond A 385:461
2. König W, Wemhöner J (1989) Ceram Bull 68:545
3. Alfaro E, Guiheen J, Varner JR (1990) In: Fréchette VD, Varner JR (eds) Fractography of glasses and ceramics. Ceramic transactions, vol 17. The American Ceramic Society, Ohio, p 485

4. Frei H, Grathwohl G (1993) Ceram Int 19:93
5. Cho S, Huh Y, Yoon K (1994) J Am Ceram Soc 77:2443
6. Olsson M, Kahlman L, Nyberg B (1995) Am Ceram Soc Bull 74:48
7. Xu HHK, Wei L, Jahanmir S (1996) J Am Ceram Soc 79:1307
8. Tonshoff HK, Lierse T, Wobker HG (1997) Ceram Ind 15:193
9. Li K, Liao W (1996) J Mater Proc Technol 57:207
10. Tomba Martinez AG, Cavalieri AL (2000) Mat Res Bull 35:1077
11. Tomba Martinez AG, Cavalieri AL (2000) J Eur Ceram Soc 20:889
12. Lange FF, Gupta TK (1970) J Am Ceram Soc 53:54
13. Gupta TK (1976) J Am Ceram Soc 59:259
14. Chou IA, Chan H, Harmer MP (1996) J Am Ceram Soc 79:2403
15. Seidel J, Calussen N, Rödel J (1997) J Eur Ceram Soc 17:727
16. Leoni M, Scardi P, Sglavo V (1998) J Eur Ceram Soc 18:1663
17. Pfeiffer W, Hollstein T (1997) J Eur Ceram Soc 17:487
18. Lutterotti L, Scardi P (1990) J Appl Cryst 23:246
19. Standard practice for fractography and characterization of fracture origins in advanced ceramics, ASTM-C 1322/96
20. Brinksmeier E, Siemer H (1989) In: International conference on residual stresses (ICRS2) proceedings, Nancy, France, 23–25 November 1989, p 335
21. Watchman JB Jr, Teft WE, Lam DG Jr, Stinchfield RP (1960) J Am Ceram Soc 45:319
22. Tomba Martinez AG, Cavalieri AL (2002) J Am Ceram Soc 85:921
23. Eigenmann B, Scholtes B, Macherauch E (1989) Mater Sci Eng A 118:1
24. Wu HZ, Roberts SG, Möbus G, Inkson BJ (2003) Acta Mater 51:149
25. Wu H, Roberts SG, Derby B (2001) Acta Mater 49:507
26. Choi S, Awaji H (2005) Sci Technol Adv Mater 6:2
27. Cannon RM, Rhodes WH, Heuer AH (1980) J Am Ceram Soc 63:46
28. Gitzen WH (1970) Alumina as ceramic material. The American Ceramic Society, Ohio
29. Munro R (1997) J Am Ceram Soc 80:1919
30. González ES, Miranda P, Martínez JJM, Guiberteau F, Pajares A (2007) J Eur Ceram Soc 27:3345
31. Cook RF, Lawn BR, Dabbs TP, Chantikul P (1981) J Am Ceram Soc 64:C121
32. Lange FF, James MR, Green DJ (1983) J Am Ceram Soc 66:C16
33. Swab JJ, Quinn GD (1995) Report No. 19, ISSN 1016-2186
34. Rice RW (1994) J Am Ceram Soc 77:2232
35. Augusto Lino UR, Hüber HW (1983) In: Science of ceramics 12, Ceramurgica s.r.l. (Faenza), p 607
36. Samuel R, Chandrasekar S, Farris T, Licht R (1989) J Am Ceram Soc 72:1960
37. Zhao J, Stearns L, Harmer M, Chan H, Miller G (1993) J Am Ceram Soc 76:503
38. Tomba Martinez AG, Cavalieri AL (2000) Mater Lett 42:240
39. Tomba Martinez AG, Cavalieri AL (2000) Mater Sci Eng A 276:76
40. Tomba Martinez AG, Camerucci MA, Cavalieri AL (2006) J Eur Ceram Soc 26:2527
41. Xu HHK, Jahanmir S (1995) J Mater Sci 30:2235. doi:10.1007/BF01184566
42. Pfeiffer W, Frey T (2006) J Eur Ceram Soc 26:2639